Analytical and Bioanalytical Chemistry
https://doi.org/10.1007/s00216-023-04890-6

RESEARCH PAPER

High-throughput analysis of lipidomic phenotypes of methicillin-resistant *Staphylococcus aureus* by coupling in situ 96-well cultivation and HILIC-ion mobility-mass spectrometry

Rutan Zhang[1] · Nate K. Ashford[2] · Amy Li[1] · Dylan H. Ross[1,3] · Brian J. Werth[2] · Libin Xu[1]

Received: 21 July 2022 / Revised: 23 July 2023 / Accepted: 25 July 2023

Abstract

Antimicrobial resistance is a major threat to human health as resistant pathogens spread globally, and the development of new antimicrobials is slow. Since many antimicrobials function by targeting cell wall and membrane components, high-throughput lipidomics for bacterial phenotyping is of high interest for researchers to unveil lipid-mediated pathways when dealing with a large number of lab-selected or clinical strains. However, current practice for lipidomic analysis requires the cultivation of bacteria on a large scale, which does not replicate the growth conditions for high-throughput bioassays that are normally carried out in 96-well plates, such as susceptibility tests, growth curve measurements, and biofilm quantitation. Analysis of bacteria grown under the same condition as other bioassays would better inform the differences in susceptibility and other biological metrics. In this work, a high-throughput method for cultivation and lipidomic analysis of antimicrobial-resistant bacteria was developed for standard 96-well plates exemplified by methicillin-resistant *Staphylococcus aureus* (MRSA). By combining a 30-mm liquid chromatography (LC) column with ion mobility (IM) separation, elution time could be dramatically shortened to 3.6 min for a single LC run without losing major lipid features. Peak capacity was largely rescued by the addition of the IM dimension. Through multi-linear calibration, the deviation of retention time can be limited to within 5%, making database-based automatic lipid identification feasible. This high-throughput method was further validated by characterizing the lipidomic phenotypes of antimicrobial-resistant mutants derived from the MRSA strain, W308, grown in a 96-well plate.

Keywords Lipidomics · Bacteria · Antimicrobial resistance · High throughput · Ion mobility-mass spectrometry

Introduction

Antimicrobial resistance (AMR) among bacterial pathogens is a significant threat to public health around the world [1]. Methicillin-resistant *Staphylococcus aureus* (MRSA) represents such a pathogen, causing more than 120,000 deaths per year globally [2]. Cell envelope-targeting antimicrobials, such as vancomycin, dalbavancin, and daptomycin, represent major classes of drugs against bacterial pathogens, and resistance to these drugs often results in altered cell membrane and cell wall metabolism [3–7]. As such, lipidomic analysis characterizing altered lipid metabolism among such pathogens is crucial for understanding the relationship between membrane composition and AMR phenotypes [5, 7–9]. Nevertheless, high-throughput analytical techniques for lipidomic analysis are still challenging due to the extreme structural diversity of lipids in biological samples and large differences in the physicochemical properties of individual lipid species [10, 11].

Classical lipidomic strategies include the direct infusion shotgun mass spectrometry (MS) approach and the liquid chromatography (LC)-MS approach [10–16]. The shotgun MS method is considered to be high-throughput and is mostly based on triple quadrupole or quadrupole-linear ion trap instruments [12, 13]. However, this method is less effective in direct resolving isobaric and isomeric species

✉ Libin Xu
libinxu@uw.edu

[1] Department of Medicinal Chemistry, University of Washington, Seattle, WA 98195, USA

[2] Department of Pharmacy, University of Washington, Seattle, WA 98195, USA

[3] Present Address: Biological Sciences Division, Pacific Northwest National Laboratory, WA 99352 Richland, USA

Published online: 03 August 2023

and tends to lose sensitivity for those low-abundance species due to their low resolution and possible ion suppression [16]. High-resolution mass spectrometers have been employed to improve the selectivity, accuracy, and coverage of the shotgun lipidomics [17, 18]. The LC–MS method has better resolving power but is typically more time-consuming with the analysis time in tens of minutes to hours [11, 14, 15]. This method also faces challenges in separating most of the isomeric species at the LC chromatographic peak level without using special columns, like chiral, SFC, or 2D-LC [19]. Most recently, supercritical fluid chromatography (SFC) has been proven to increase the coverage of the lipidome by a factor of 3.4 with a decrease in analysis time by 40% [18, 20].

Ion mobility (IM), a technique capable of separating ions based on their gas-phase size and shape, has found numerous applications in biomolecule analysis by integrating with MS [21–28]. A typical cycle of IM separation usually occurs in milliseconds time scale in time-dispersive traveling wave or drift tube IM instruments, making it suitable to couple with LC to provide an orthogonal separation and increase peak capacity without increasing analysis time. From IM-MS analysis, a physical property of an ion, ion-neutral collision cross sections (CCS) [19, 24, 25], can be measured, which can be used for the characterization and differentiation of structural isomers. Thus, due to its speed, sensitivity, and selectivity, IM-MS has been widely used for the analysis of small molecules [25–27, 29–32]. The hydrophilic interaction LC(HILIC)-IM-MS-based lipidomic method has been proven to be robust in resolving a large number of lipid species that occupy the narrow mass-to-charge (*m/z*) window of 600–900 [7, 19, 33].

96-well plates have been widely used in high-throughput bioassays for bacteria, such as measuring bacterial growth curves, determining minimum inhibitory concentrations (MIC), and quantitating biofilm formation [34–37] However, current practice for bacterial lipidomics requires cultivation of the bacteria on a large scale (10–30 mL or more) [7, 38], which does not replicate the growth conditions for other bioassays. Growth of bacteria in different volumes may affect physiology due to variations in environmental and physiological factors, such as cell density, nutrient and glycerol concentration, waste accumulation level, and pH changes [39]. Thus, to better correlate the lipidomic results with those of other high-throughput bioassays, cultivation under the same condition would be desired. To the best of our knowledge, the direct analysis of the lipidomes of microbes grown in 96-well plates has yet to be examined.

The objective of this study was to evaluate the feasibility of using significantly shortened HILIC-IM-MS analysis and small-volume cultivation in 96-well plates for high-through bacterial lipidomics by measuring peak capacity and investigating the lipidomic alterations between MRSA strains. The potential of this high-throughput method was further demonstrated by characterizing the lipidomic phenotype of seven W308-derived *S. aureus* mutants selected against the lipoglycopeptide, dalbavancin, and assessing the relationship between the genotype and the lipidomic phenotype.

Materials and methods

Reagents, media, and strains High-performance LC-grade solvents (water, acetonitrile, chloroform, and methanol) and ammonium acetate were purchased from Thermo Fisher Scientific. All lipid standards were purchased from Avanti Polar Lipids and prepared at 1 mM in chloroform for stocks and then diluted to 5 µM prior to LC–MS analysis. Brain heart infusion (BHI) broth was used to culture organisms prior to lipidomic analysis. The well-characterized USA300 MRSA strain, JE2, was acquired from BEI Resources, and an isogenic daptomycin-nonsusceptible strain, JE2-Dap2, was selected against daptomycin pressure as described previously [5]. W308 is a clinical MRSA isolate that is part of the Werth Lab strain collection, and dalbavancin-nonsusceptible strains derived from W308 were selected by in vitro pharmacokinetic/pharmacodynamic modeling simulating clinical dalbavancin exposures as described previously [40].

Cultivation of MRSA Parent JE2 and JE2-Dap2 strains were grown at 37 °C overnight in 200 µL and 30 mL of BHI broth in 96-well plates and 50-mL tubes, respectively, with shaking at 120 rpm. W308 strain series were grown in 200 µL of BHI broth in 96-well plates under the same condition. After overnight cultivation, bacterial broth from 96-well plates was transferred into 1.5-mL Eppendorf tubes. All suspensions from both the small and large-scale growth were then pelleted by centrifugation, washed with 1 × PBS buffer, and then subjected to lipid extraction.

Extraction of lipids in *S. aureus* Lipid extraction was performed using the methyl-tert-butyl ether (MTBE)-based lipid extraction method. Briefly, 50 µL of chilled water was added to the pelleted bacteria. After vortexing briefly, the suspension was subjected to sonication in ice bath for 30 min to dislodge pellets from the tube. Three hundred microliters of chilled methanol, 500 µL of MTBE, and 4 µL of 62.5 µM internal standards mixture were then added to each tube consecutively. The samples were vortexed vigorously for 10 min. 250 µL of chilled water was added to each tube. After brief vortexing again, the samples were centrifuged for 10 min at 4 °C and 2000 × *g*. The upper phase was then collected into a new 1.5-mL Eppendorf tube and dried in a vacuum concentrator. Dried extracts were reconstituted with 100 µL of acetonitrile/methanol (2:1) for LC–MS analysis. Four commercial synthetic lipids, i.e., CL 14:1, MGDG 18:1, LysylPG

18:1, and PG 18:1, were chosen as internal standards to measure the absolute quantities of each lipid species because *S. aureus* only produce saturated lipids endogenously. The ESI response factor between DGDG 18:0 and MGDG 18:1 was measured and used to quantify all DGDGs.

HILIC-IM-MS method LC separation was performed by a Waters Acquity FTN UPLC (Waters Corp., Milford, MA) with the column and autosampler temperature maintained at 40 °C and 4 °C, respectively, and the flow rate at 0.5 mL/min. The mobile phases consisted of (A) acetonitrile/water (50:50) and (B) acetonitrile/water (95:5), both containing 5 mM ammonium acetate. Five microliter and 10 µL of samples were injected for positive- and negative-mode analyses, respectively. For bacterial lipid analysis with three different gradients, a Phenomenex Kinetex HILIC column (100 × 2.1 mm, 1.7 µm) was employed, and three gradient elution programs were as follows: (1) 0–1 min, 100% B; 1–4 min, 100–90% B; 4–7 min, 90–70% B; 7–8 min, 70% B; 8–9 min, 70–100% B, 9–12 min, 100%B; (2) 0–0.8 min, 100% B; 0.8–1.8 min, 100–90% B; 1.8–2.8 min, 90–70% B; 2.8–3.8 min, 70% B; 3.8–4.8 min, 70–100% B, 4.8–8 min, 100%B; (3) 0–2 min, 100% B; 2–8 min, 100–90% B; 8–14 min, 90–70% B; 14–15 min, 70% B; 15–16 min, 70–100% B, 16–19 min, 100%B. For bacterial lipid analysis using three different columns, in addition to above 100-mm column, a 50-mm (Phenomenex Kinetex, 50 × 2.1 mm, 1.7 µm) and a 30-mm (Phenomenex Kinetex, 30 × 2.1 mm, 1.7 µm) column were used. The gradients for different columns were changed proportionally in linear relation to their lengths. Specifically, the gradients for 50-mm and 30-mm columns were as follows: (1) 0–0.5 min, 100% B; 0.5–2 min, 100–90% B; 2–3.5 min, 90–70% B; 3.5–4 min, 70% B; 4–4.5 min, 70–100% B, 4.5–6 min, 100%B; (2) 0–0.3 min, 100% B; 0.3–1.2 min, 100–90% B; 1.2–2.1 min, 90–70% B; 2.1–2.4 min, 70% B; 2.4–2.7 min, 70–100% B, 2.7–3.6 min, 100%B.

IM-MS analysis was performed on a Waters Synapt G2-Si ion mobility-mass spectrometer and run in HDMS^E mode with parameters optimized as follows: (1) MS ion spray voltages in positive and negative modes were + 2500 V and − 2000 V, respectively; scan range, 50–1200 m/z; traveling-wave velocity and height, 500 m/s and 40 V; (2) MS/MS collision energy ramped from 25 to 45 eV.

Calculation of peak capacity Peak capacity, P_c, is a quantitative measure of the theoretical maximum peaks available from a gradient separation [32]. Same as the LC separation, the P_c of IM can be calculated based on the following equation (Eq. 1) [32, 41, 42]:

$$P_c = \frac{t_{max} - t_{min}}{0.5 \times \left(w_{max} + w_{min}\right)} \quad (1)$$

where t_{max} and t_{min} are the drift times of the slowest and fastest ions and w_{max} and w_{min} are the widest and narrowest full width at half maximum of the ion peaks. Therefore, the P_c of the hybrid two-dimensional separation, LC-IM, can be calculated from $P_c(LC - IM) = P_c(LC) \times P_c(IM)$.

Data analysis Data alignment, peak picking, and normalization were performed by the Progenesis QI (Waters Corp.). A pooled sample was designated as the alignment reference. The default "all compounds normalization" was applied to correct the variation of total ion current (TIC) among different samples. For absolute quantification, the ratio between each lipid species and the corresponding internal standard of the same lipid class was calculated based on the raw data. Lipids were annotated using a combination of an open-source Python package, *LiPydomics* [43], with a built-in lipid database and manual examination based on an in-house version of LipidPioneer modified to contain the major lipid species observed in *S. aureus* [5, 44]. The linearity and LOQ of absolute quantification were measured and listed in Table S1. Heatmap and partial least squares (PLS) regression analysis were performed using the ClustVis web tool and Origin Lab, respectively.

Results and discussion

Effect of the short columns on peak capacity To evaluate the impact of the length of HILIC columns on peak capacity in separating lipids, lipid extracts from a large-scale (30 mL) growth of the well-documented JE2 strain were chosen as a benchmark. From our previous research on the lipidome of *S. aureus*, it is known that the earliest eluted lipid under the HILIC condition is DGDG 37:0, while the last eluted lipid is LysylPG 29:0 [7]. The base peak chromatograms were shown in Fig. S1. FWHMs (full width at half maximum) were recorded from replotted chromatographic peaks using Gaussian fitting in OriginPro software (OriginLab Corporation, Northampton, MA). Therefore, the peak capacity within the time period defined by these two lipids can be calculated using Eq. 1.

As shown in Fig. 1A and B, peak capacity drastically declined as the column length decreased to 50 mm and 30 mm, which could be accounted for by the decreased number of the theoretical plates according to the plate-height equation [45, 46], HETP = L / N, where HETP stands for the height equivalent to a theoretical plate, *L* refers to column length, and *N* refers to the number of theoretical plates. However, the peak width tends to become much narrower when a short column is used due to lesser molecular diffusion and Eddy diffusion [46], which was exemplified by the non-linear decline of peak capacity from 100 to 30 mm. In addition, to avoid overloading of analytes in short columns, ½ and 1/3 of the injection volume were tested on the

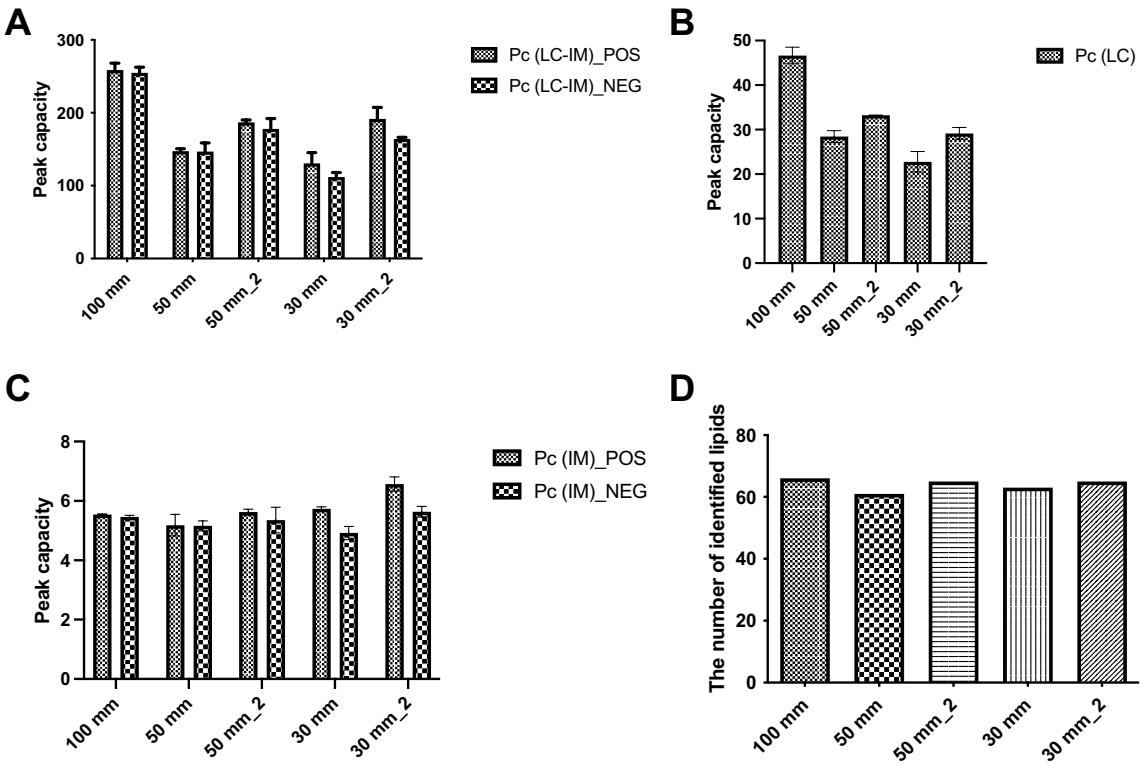

Fig. 1 **A**–**C** Peak capacity of HILIC-IM, LC, and IM in separating bacterial lipids and **D** the number of identified lipids in JE2 MRSA under various chromatography conditions

50-mm- and 30-mm columns (50 mm_2 and 30 mm_2 in Fig. 1A and B), respectively. As expected, both peak capacities increased, even with the shortest 30-mm column, peak capacity within the chromatographic region from DGDG 37:0 to Lysyl-PG 29:0 was comparable to that of the 50-mm column, which can separate more than 180 and 160 lipids in positive and negative mode, respectively. Figure 1C reveals that the peak capacity of ion mobility has no direct correlation with the changes in column length. Intriguingly, as injection volume decreased, the peak capacity of ion mobility also increased, indicating the drift tube could also be overloaded like LC. Overall, a single LC run for lipidomics could be dramatically shortened to 3.6 min, with only a small sacrifice of peak capacity compared to the 100-mm column.

In addition to the theoretical calculation of peak capacity, the real number of identified lipids in the JE2 strain was also counted based on the LiPydomics Python package [43] and our in-house lipidomic library (CCSbase.net/lipids_query). As shown in Fig. 1D, almost all known major lipids could be detected with all three columns, either with the same injection or adjusted volume, indicating that the peak capacity of the short columns is sufficient for lipidomic phenotyping of bacteria.

Comparison of absolute quantitation and all-compounds normalization on bacterial lipid profiles A JE2 strain pair from our previous research was employed to evaluate the changes in lipid phenotypes affected by variation of the cultivation condition in the 96-well plate [5]. One strain is the daptomycin-sensitive wild-type parent JE2 strain, named Par-MRSA, while the other is the JE2-derived daptomycin-resistant strain named Dap2-MRSA, which contains a mutation in *mprF* that encodes the lysyl-phosphotidylglycerol (LysylPG) synthase. The accuracy of internal standards-based absolute quantification was evaluated (Table S1), with R^2 of the standard curves greater than 0.95 for all four main lipid classes, i.e., CLs, DGDGs, LysylPGs, and PGs. As shown in Fig. 2, the general trend of the alteration of four main lipid classes in Dap2-MRSA versus Par-MRSA was highly consistent between the absolute quantitation (Fig. 2A) and the all-compounds normalization result (Fig. 2B), demonstrating the robustness of all compounds normalization, at least in analyzing MRSA lipids obtained using the 96-well plate. The ratio of each lipid species between Dap2-MRSA and Par-MRSA was also calculated and visualized in Figure S2 in Electronic Supplementary Material, further confirming that both approaches worked nearly identically in capturing lipid profile alterations between the strain pair. Importantly, in comparison with the lipidomic results we

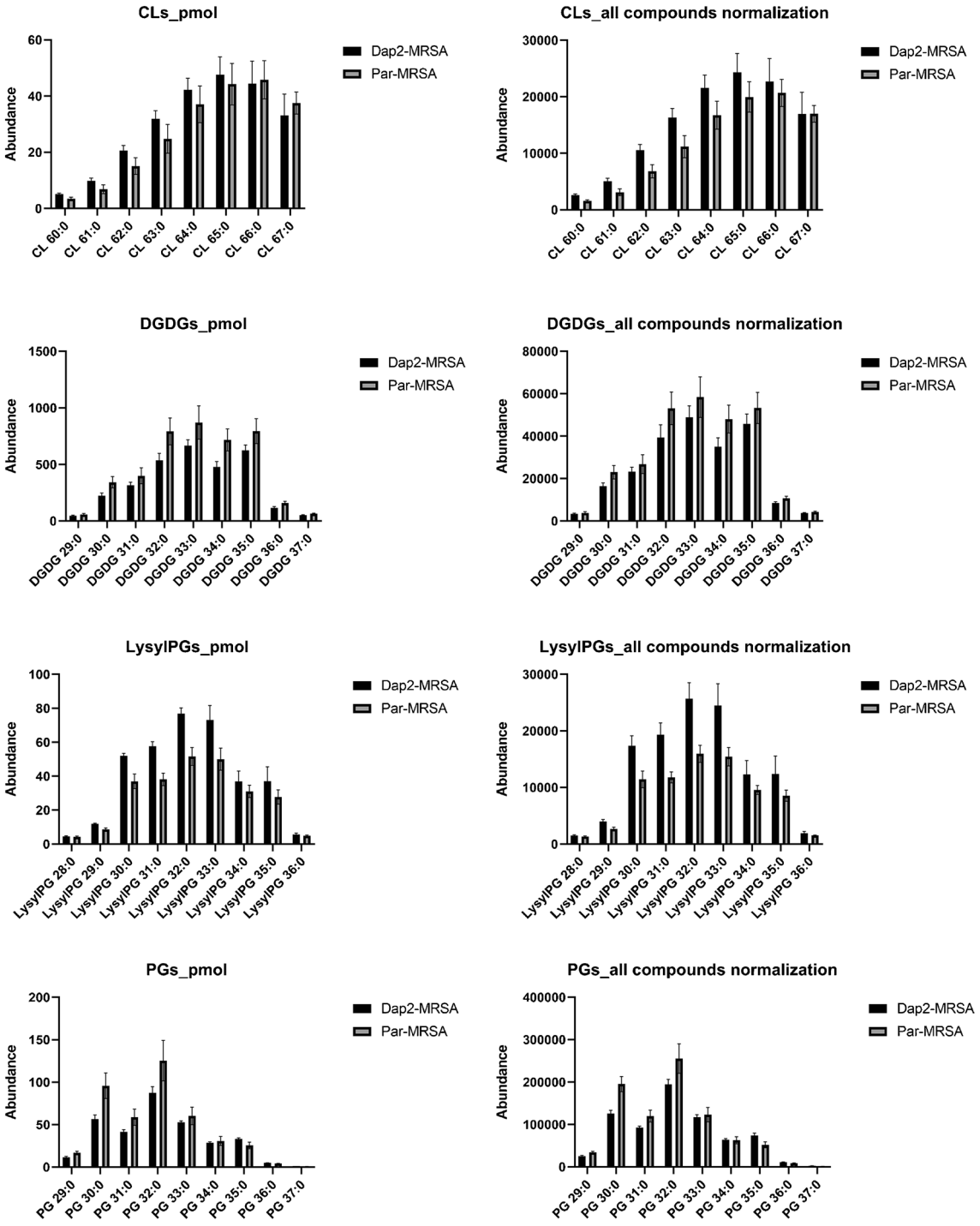

Fig. 2 The abundance of lipids profiles in Dap2-MRSA and Par-MRSA grown in 96-well plates by absolute quantitation in pmol (**A**) and all-compound normalization (**B**)

reported previously [5], the general trends of the alterations of four main lipid classes, i.e., CLs (increases), DGDGs (decreases), LysylPGs (increases), and PGs (decreases), in Dap2-MRSA versus Par-MRSA were similar, but the extent of changes was different, which could be partly due to microbial physiological changes as a result of the variation of incubation conditions (confined 96-well plate incubation vs. 25-mL large scale incubation) [39]. This finding suggests that 96-well plates-based lipidomics is necessary in order to obtain robust and accurate bioinformatic results when comparing multiple phenotypes measured using 96-well-based assays.

Calibration of retention time for automatic lipid identification To be able to automatically identify unknown lipids using our multi-dimensional (i.e., *m/z*, rt, and CCS) lipid database [43], the variation in retention time caused by the implementation of different columns and gradients needs to be eliminated. On the basis of HILIC separation, the same class of lipids is typically eluted out of the column at a similar gradient region due to their same headgroup and thus similar affinities to the column [26]. Therefore, a multi-linear fitting targeting specific lipid species could be used for calibration of retention times obtained using short columns with a proportional elution gradient. As shown in Fig. 3A, retention times from both 50-mm (triangle spots) and 30-mm columns (circle spots) can be easily calibrated to the retention times in our database (obtained from 100-mm column). We note that the errors for the calibrated retention times of CLs (light blue triangles) obtained with the 50-mm column are relatively large, but they are still less than 5% (Table S1), which makes the automatic database searching feasible.

In addition, we also tested the feasibility of using a fast elution gradient on the 100-mm column. 8 min, 12 min, and 19 min gradients were tested on the basis of proportional changes of each isocratic or gradient segment, as illustrated in Fig. S3. Our results demonstrated that multiple linear interpolations were also able to accurately calibrate retention times with errors lower than 5% for these gradients (Fig. 3B, Table S3). With the retention times calibrated, lipid identification can be carried out automatically using the Python package *LiPydomics* [43], further enabling high-throughput lipidomics.

Application of high-throughput lipidomic method in measuring lipidomic phenotypes of MRSA mutants To demonstrate the utility of the high-throughput lipidomics method, we analyzed seven dalbavancin-selected strains from the MRSA W308 along with the parent strain in quadruplicates. Gene mutations of the selected strains have been characterized by whole genome sequencing as reported previously (Supplementary Table S4) [40]. The majority of the mutants carry a mutation in *walK* (but different types of mutations), which encodes part of the essential two-component system, WalKR, that regulates cell wall metabolism [47, 48] and central metabolism [49]. A mutation in *walR* was also observed in one strain (W308-336B). Three out of the 7 mutants also contain a mutation in *apt*, which encodes adenine phosphoribosyltransferase in the adenosyl monophosphate salvage pathway. Two strains contain a mutation in *ktrD*, which encodes Ktr system potassium uptake protein D that is important for resistance to osmotic stress [50]. One strain contains a mutation in *stp1*, which was suggested to regulate *walR* phosphorylation [51–53]. The lipidomic results (Fig. 4) suggest that the presence of *walK* mutation alone (W308-504B) results in significantly decreased levels of CLs, lysylPGs, and DGDGs, whereas the presence of *walR* alone (W308-336B) results in significantly increased levels of all four lipid classes. PLS regression analysis was carried out to evaluate the contribution of various mutations to the lipid profiles (Fig. S4), which showed that mutations in *walK* or *stp1* have a negative correlation with lipid levels while mutations in *walR*, *apt*, *ktrD*, and *clp-like protease* have a generally positive correlation with lipid levels.

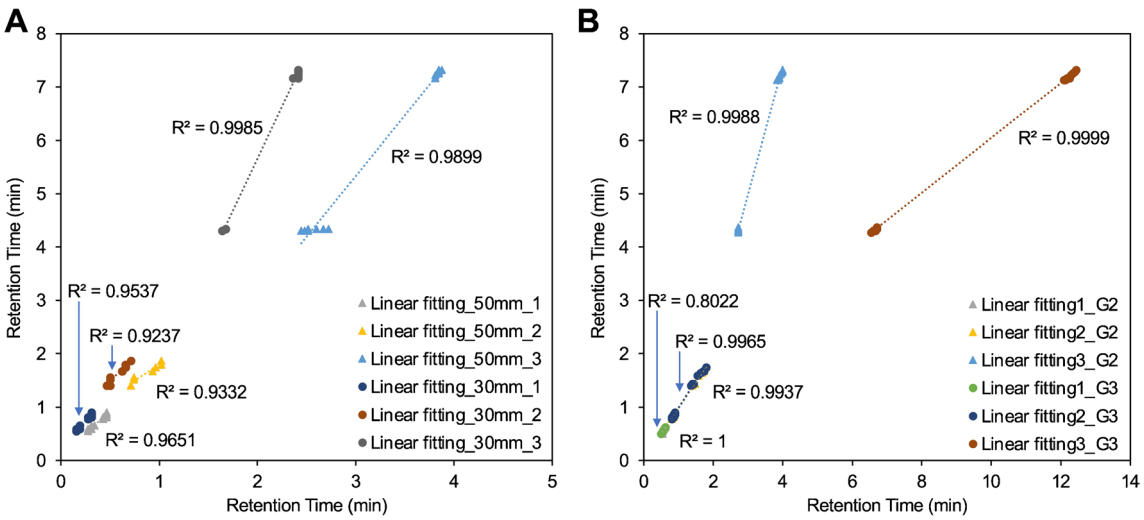

Fig. 3 **A** Calibration of retention times of lipids obtained with 30-mm and 50-mm columns to retention times of lipids obtained from 100-mm column. *Y*-axis represented the retention times measured with the 100-mm column, while *X*-axis represented the retention times measured with the 50-mm (triangle spots) or 30-mm (circle spots) column. **B** Calibration of retention times obtained with different gradients. *Y*-axis represented the retention times measured with gradient 1, while *X*-axis represented the retention times measured with gradient 2 (triangle spots) or gradient 3 (circle spots). Linear fitting curves 1, 2, and 3 indicated fitting of retention times of FFAs and DGDGs, PGs, and CLs and LysylPGs, respectively

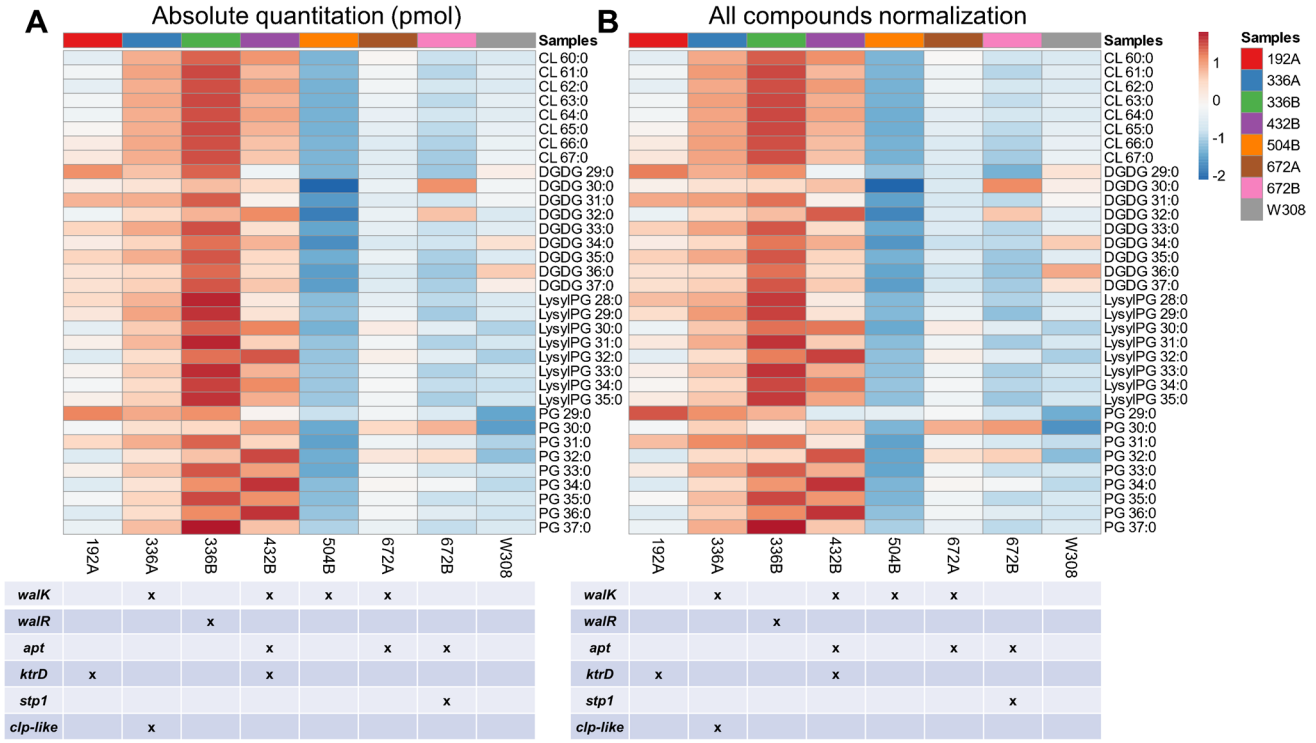

Fig. 4 Heatmap of lipid profiles with absolutation quantitation (**A**) or all-compounds normalization (**B**) of seven W308 mutants in comparison with W308 wild-type strain. $N=4$ per group. Averaged values presented. "x" in the table below marks the presence of a mutation in the specific gene

Among strains containing a mutation in *walK*, mutations in *clp-like protease* (W308-336A), *ktrD* (W308-432B), or *apt* (W308-672A) could somehow counter the lipid variations induced by *walK* (Fig. 4), which were also consistent with the PLS coefficients variation (Figure S4). These results suggest that mutations in *clp-like protease*, *ktrD*, or *apt* could be compensatory mutations that improve the fitness of the *walK* mutants. Thus, the small-scale cultivation and high-throughput lipidomic method was able to capture significant lipidomic changes resulting from drug resistance-associated mutations, which paves the way for the application of this strategy in the metabolic phenotyping of a large number of lab-derived and clinical bacterial strains.

Conclusion

We developed and evaluated a short column-based multi-dimensional HILIC-IM-MS lipidomics method in combination with a 96-well plate-based bacterial cultivation method to achieve high-throughput lipidomic analysis of large-scale antimicrobial-resistant microbes. We found that while shorter LC runs result in a slightly reduced capacity in the LC dimension, the peak capacity in the IM dimension was not affected. As a result, a single LC run could be shortened to 3.6 min without losing major lipid species, with peak capacities of up to 180 and 162 lipids for positive and negative modes, respectively. The deviation of retention time caused by the implementation of different columns or gradients could be easily calibrated based on multiple linear interpolations with a calibration error of less than 5%, which enables automatic lipid identification using *LiPydomics* with manual supervision. 96-well plate-based high-throughput cultivation displayed distinct lipid profiles from that obtained by large-scale cultivation, demonstrating the necessity of performing small-scaled lipidomics especially when correlating with phenotypes obtained using other 96-well plate-based assays. Further studies on dalbavancin-selected W308 strain mutants exemplified that major differences in lipid profiles among different strains could be captured, which makes this method suitable for rapid phenotyping of a large number of strains in parallel with other high-throughput bioassays. Overall, this high-throughput bacterial lipidomic method could be useful for reliable large-scale surveillance studies where multiple 96-well plate-based biochemical assays are needed or could establish the foundation for a clinical diagnostic tool to guide practice.

Supplementary Information The online version contains supplementary material available at https://doi.org/10.1007/s00216-023-04890-6.

Author contribution L. Xu and R. Zhang contributed to the study conception and design. Material preparation, data collection, and analysis

were performed by R. Zhang, N.K. Ashford, A. Li, and D.H. Ross. The first draft of the manuscript was written by R. Zhang with contributions from L. Xu and B.J. Werth. All authors read and approved the final manuscript.

Funding This work was supported by the National Institute of Allergy and Infectious Diseases of the National Institutes of Health under award number R01AI136979.

Declarations

Conflict of interest The authors declare no competing interests.

References

1. Dadgostar P. Antimicrobial resistance: implications and costs. Infect Drug Resist. 2019;12:3903–10.
2. Antimicrobial Resistance C. Global burden of bacterial antimicrobial resistance in 2019: a systematic analysis. Lancet. 2022;399:629–55.
3. Khan A, Davlieva M, Panesso D, Rincon S, Miller WR, Diaz L, Reyes J, Cruz MR, Pemberton O, Nguyen AH, Siegel SD, Planet PJ, Narechania A, Latorre M, Rios R, Singh KV, Ton-That H, Garsin DA, Tran TT, Shamoo Y, Arias CA. Antimicrobial sensing coupled with cell membrane remodeling mediates antibiotic resistance and virulence in Enterococcus faecalis. Proc Natl Acad Sci U S A. 2019;116:26925–32.
4. Jiang JH, Bhuiyan MS, Shen HH, Cameron DR, Rupasinghe TWT, Wu CM, Le Brun AP, Kostoulias X, Domene C, Fulcher AJ, McConville MJ, Howden BP, Lieschke GJ, Peleg AY. Antibiotic resistance and host immune evasion in Staphylococcus aureus mediated by a metabolic adaptation. Proc Natl Acad Sci U S A. 2019;116:3722–7.
5. Hines KM, Shen T, Ashford NK, Waalkes A, Penewit K, Holmes EA, McLean K, Salipante SJ, Werth BJ, Xu L. Occurrence of cross-resistance and beta-lactam seesaw effect in glycopeptide-, lipopeptide- and lipoglycopeptide-resistant MRSA correlates with membrane phosphatidylglycerol levels. J Antimicrob Chemother. 2020;75:1182–6.
6. Bayer AS, Schneider T, Sahl HG. Mechanisms of daptomycin resistance in Staphylococcus aureus: role of the cell membrane and cell wall. Ann N Y Acad Sci. 2013;1277:139–58.
7. Hines KM, Waalkes A, Penewit K, Holmes EA, Salipante SJ, Werth BJ, Xu L. Characterization of the mechanisms of daptomycin resistance among gram-positive bacterial pathogens by multidimensional lipidomics. mSphere. 2017;2:e00492-00417.
8. Hewelt-Belka W, Nakonieczna J, Belka M, Baczek T, Namiesnik J, Kot-Wasik A. Untargeted lipidomics reveals differences in the lipid pattern among clinical isolates of Staphylococcus aureus resistant and sensitive to antibiotics. J Proteome Res. 2016;15:914–22.
9. Lee TH, Hofferek V, Separovic F, Reid GE, Aguilar MI. The role of bacterial lipid diversity and membrane properties in modulating antimicrobial peptide activity and drug resistance. Curr Opin Chem Biol. 2019;52:85–92.
10. Lisa M, Holcapek M. High-throughput and comprehensive lipidomic analysis using ultrahigh-performance supercritical fluid chromatography-mass spectrometry. Anal Chem. 2015;87:7187–95.
11. Quehenberger O, et al. Lipidomics reveals a remarkable diversity of lipids in human plasma. J Lipid Res. 2010;51:3299–305.
12. Han X, Gross RW. Shotgun lipidomics: electrospray ionization mass spectrometric analysis and quantitation of cellular lipidomes directly from crude extracts of biological samples. Mass Spectrom Rev. 2005;24:367–412.
13. Schwudke D, Liebisch G, Herzog R, Schmitz G, Shevchenko A. Shotgun lipidomics by tandem mass spectrometry under data-dependent acquisition control. Methods Enzymol. 2007;433:175–91.
14. Merrill AH Jr, Sullards MC, Allegood JC, Kelly S, Wang E. Sphingolipidomics: high-throughput, structure-specific, and quantitative analysis of sphingolipids by liquid chromatography tandem mass spectrometry. Methods. 2005;36:207–24.
15. Ivanova PT, Milne SB, Byrne MO, Xiang Y, Brown HA. Glycerophospholipid identification and quantitation by electrospray ionization mass spectrometry. Methods Enzymol. 2007;432:21–57.
16. Hu CF, Duan Q, Han XL. Strategies to Improve/Eliminate the Limitations in Shotgun Lipidomics. Proteomics. 2020;20:e1900070.
17. Eggers LF, Schwudke D. Shotgun lipidomics approach for clinical samples. In: Giera M (ed) Clinical Metabolomics: Methods and Protocols. Springer New York, New York, NY, pp 163-174. 2018. https://doi.org/10.1007/978-1-4939-7592-1_12.
18. Kofeler HC, Ahrends R, Baker ES, Ekroos K, Han XL, Hoffmann N, Holcapek M, Wenk MR, Liebisch G. Recommendations for good practice in MS-based lipidomics. J Lipid Res. 2021;62:100138.
19. Hines KM, May JC, McLean JA, Xu L. Evaluation of Collision Cross Section Calibrants for Structural Analysis of Lipids by Traveling Wave Ion Mobility-Mass Spectrometry. Anal Chem. 2016;88:7329–36.
20. Lisa M, Cifkova E, Khalikova M, Ovcacikova M, Holcapek M. Lipidomic analysis of biological samples: comparison of liquid chromatography, supercritical fluid chromatography and direct infusion mass spectrometry methods. J Chromatogr A. 2017;1525:96–108.
21. Kim HI, Kim H, Pang ES, Ryu EK, Beegle LW, Loo JA, Goddard WA, Kanik I. Structural characterization of unsaturated phosphatidylcholines using traveling wave ion mobility spectrometry. Anal Chem. 2009;81:8289–97.
22. Jackson SN, Ugarov M, Post JD, Egan T, Langlais D, Schultz JA, Woods AS. A study of phospholipids by ion mobility TOFMS. J Am Soc Mass Spectrom. 2008;19:1655–62.
23. Kliman M, May JC, McLean JA. Lipid analysis and lipidomics by structurally selective ion mobility-mass spectrometry. Biochim Biophys Acta, Mol Cell Biol Lipids. 2011;1811:935–45.
24. May JC, McLean JA. Ion mobility-mass spectrometry: time-dispersive instrumentation. Anal Chem. 2015;87:1422–36.
25. May JC, Goodwin CR, Lareau NM, Leaptrot KL, Morris CB, Kurulugama RT, Mordehai A, Klein C, Barry W, Darland E, Overney G, Imatani K, Stafford GC, Fjeldsted JC, McLean JA. Conformational ordering of biomolecules in the gas phase: nitrogen collision cross sections measured on a prototype high resolution drift tube ion mobility-mass spectrometer. Anal Chem. 2014;86:2107–16.
26. Hines K, Herron J, Xu L. Assessment of altered lipid homeostasis by HILIC-ion mobility-mass spectrometry-based lipidomics. J Lipid Res. 2017;58:809–19.
27. Hines KM, Ross DH, Davidson KL, Bush MF, Xu L. Large-scale structural characterization of drug and drug-like compounds by high-throughput ion mobility-mass spectrometry. Anal Chem. 2017;89:9023–30.
28. Dodds JN, Baker ES. Ion mobility spectrometry: fundamental concepts, instrumentation, applications, and the road ahead. J Am Soc Mass Spectrom. 2019;30:2185–95.
29. Picache JA, Rose BS, Balinski A, Leaptrot KL, Sherrod SD, May JC, McLean JA. Collision cross section compendium to

annotate and predict multi-omic compound identities. Chem Sci. 2019;10:983–93.
30. Zheng X, Aly NA, Zhou Y, Dupuis KT, Bilbao A, Paurus VL, Orton DJ, Wilson R, Payne SH, Smith RD, Baker ES. A structural examination and collision cross section database for over 500 metabolites and xenobiotics using drift tube ion mobility spectrometry. Chem Sci. 2017;8:7724–36.
31. Ross DH, Cho JH, Xu L. Breaking down structural diversity for comprehensive prediction of ion-neutral collision cross sections. Anal Chem. 2020;92:4548–57.
32. Davidson KL, Bush MF. Effects of drift gas selection on the ambient-temperature, ion mobility mass spectrometry analysis of amino acids. Anal Chem. 2017;89:2017–23.
33. Li A, Hines KM, Xu L. Lipidomics by HILIC-ion mobility-mass spectrometry. Methods Mol Biol. 2020;2084:119–32.
34. Griffith KL, Wolf RE. Measuring beta-galactosidase activity in bacteria: cell growth, permeabilization, and enzyme assays in 96-well arrays. Biochem Biophys Res Commun. 2002;290:397–402.
35. Hazan R, Que YA, Maura D, Rahme LG. A method for high throughput determination of viable bacteria cell counts in 96-well plates. Bmc Microbiol. 2012;12:259.
36. Kensy F, Zang E, Faulhammer C, Tan RK, Buchs J. Validation of a high-throughput fermentation system based on online monitoring of biomass and fluorescence in continuously shaken microtiter plates. Microb Cell Factories. 2009;8:31.
37. Musken M, Di Fiore S, Romling U, Haussler S. A 96-well-plate-based optical method for the quantitative and qualitative evaluation of Pseudomonas aeruginosa biofilm formation and its application to susceptibility testing. Nat Protoc. 2010;5:1460–9.
38. Hines KM, Alvarado G, Chen X, Gatto C, Pokorny A, Alonzo F 3rd, Wilkinson BJ, Xu L. Lipidomic and ultrastructural characterization of the cell envelope of Staphylococcus aureus grown in the presence of human serum. mSphere. 2020;5:e00339-00320.
39 Atolia E, Cesar S, Arjes HA, Rajendram M, Shi H, Knapp BD, Khare S, Aranda-Diaz A, Lenski RE, Huang KC. Environmental and physiological factors affecting high-throughput measurements of bacterial growth. mBio. 2020;11:e01378-01320.
40. Werth BJ, Ashford NK, Penewit K, Waalkes A, Holmes EA, Ross DH, Shen T, Hines KM, Salipante SJ, Xu L. Dalbavancin exposure in vitro selects for dalbavancin-non-susceptible and vancomycin-intermediate strains of methicillin-resistant Staphylococcus aureus. Clin Microbiol Infect. 2021;27:910.e911-910.e918.
41. Ruotolo BT, McLean JA, Gillig KJ, Russell DH. Peak capacity of ion mobility mass spectrometry: the utility of varying drift gas polarizability for the separation of tryptic peptides. J Mass Spectrom. 2004;39:361–7.
42. Ruotolo BT, Gillig KJ, Stone EG, Russell DH. Peak capacity of ion mobility mass spectrometry: separation of peptides in helium buffer gas. J Chromatogr B Analyt Technol Biomed Life Sci. 2002;782:385–92.
43. Ross DH, Cho JH, Zhang R, Hines KM, Xu L. LiPydomics: a python package for comprehensive prediction of lipid collision cross sections and retention times and analysis of ion mobility-mass spectrometry-based lipidomics data. Anal Chem. 2020;92:14967–75.
44. Ulmer CZ, Koelmel JP, Ragland JM, Garrett TJ, Bowden JA. LipidPioneer : a comprehensive user-generated exact mass template for lipidomics. J Am Soc Mass Spectrom. 2017;28:562–5.
45. Colmsjo AL, Ericsson MW. Assessment of the height equivalent to a theoretical plate in liquid-chromatography. J Chromatogr. 1987;398:63–71.
46. Lundanes E, Lo R, Greibrokk T. Chromatography: basic principles, sample preparations and related methods. Weinheim, Germany: Wiley-VCH Verlag GmbH & Co. KGaA; 2014.
47. Dubrac S, Msadek T. Identification of genes controlled by the essential YycG/YycF two-component system of Staphylococcus aureus. J Bacteriol. 2004;186:1175–81.
48. Dubrac S, Boneca IG, Poupel O, Msadek T. New insights into the WalK/WalR (YycG/YycF) essential signal transduction pathway reveal a major role in controlling cell wall metabolism and biofilm formation in Staphylococcus aureus. J Bacteriol. 2007;189:8257–69.
49. Howden BP, McEvoy CR, Allen DL, Chua K, Gao W, Harrison PF, Bell J, Coombs G, Bennett-Wood V, Porter JL, Robins-Browne R, Davies JK, Seemann T, Stinear TP. Evolution of multidrug resistance during Staphylococcus aureus infection involves mutation of the essential two component regulator WalKR. PLoS Pathog. 2011;7: e1002359.
50. Gries CM, Bose JL, Nuxoll AS, Fey PD, Bayles KW. The Ktr potassium transport system in Staphylococcus aureus and its role in cell physiology, antimicrobial resistance and pathogenesis. Mol Microbiol. 2013;89:760–73.
51. Cheung A, Duclos B. Stp1 and Stk1: the Yin and Yang of vancomycin sensitivity and virulence in vancomycin-intermediate Staphylococcus aureus strains. J Infect Dis. 2012;205:1625–7.
52. Cameron DR, Ward DV, Kostoulias X, Howden BP, Moellering RC Jr, Eliopoulos GM, Peleg AY. Serine/threonine phosphatase Stp1 contributes to reduced susceptibility to vancomycin and virulence in Staphylococcus aureus. J Infect Dis. 2012;205:1677–87.
53. Libby EA, Goss LA, Dworkin J. The eukaryotic-like Ser/Thr kinase PrkC regulates the essential WalRK two-component system in Bacillus subtilis. PLoS Genet. 2015;11: e1005275.